THE JOURNAL OF PHYSICAL CHEMISTRY C

Article

pubs.acs.org/JPCC

CVD Graphene Transferred with Au Nanoparticles: An Ideal Platform for TERS and SERS on a Single Triangular Nanoplate

Luis A. Pérez,[‡] María C. Dalfovo,[†] Horacio Troiani,[§] Analía L. Soldati,[§] Gabriela I. Lacconi,*[,‡] and Francisco J. Ibañez*[,†]

[†]Instituto de Investigaciones Fisicoquímicas, Teóricas y Aplicadas (INIFTA), Universidad Nacional de La Plata - CONICET, Sucursal 4 Casilla de Correo 16, (1900) La Plata, Argentina

[‡]INFIQC-CONICET, Dpto. de Fisicoquímica, Facultad de Ciencias Químicas, Universidad Nacional de Córdoba, Ciudad Universitaria, (5000) Córdoba, Argentina

[§]Centro Atómico Bariloche, Consejo Nacional de Investigaciones Científicas y Técnicas (CONICET), Av. Bustillo 9500, S.C. de Bariloche, CP 8400 Rio Negro, Argentina

Supporting Information

ABSTRACT: Transferring CVD graphene using surfactant-protected Au nanoparticles (Au NPs) avoids the use of PMMA and opens new ways of building heterojunctions for TERS and SERS applications. Thermal treatment removes organics from the Au NPs and leads to larger nanoparticles and the formation of networks, dimmers, and nanoplates of various shapes (circles, hexagons, and triangles). Raman and HRTEM revealed bilayer graphene and Moiré patterns as determined by the 2D band and dislocated atomic layers, respectively. TERS performed on the heterojunction exhibits a reversible increase in frequency and sharpening of the characteristic bands in graphene along with the exaltation of bands such as D + D′. A close examination into a single triangular-shape nanoplate reveals that the most irregular area of the nanoplate is consistent with the higher Raman enhancement of Rh6G when compared to other areas of the same feature. This work may shed light onto new ways of transferring graphene, fundamental aspects concerning local strains in the heterojunction, and SERS on a single Au nanostructure.

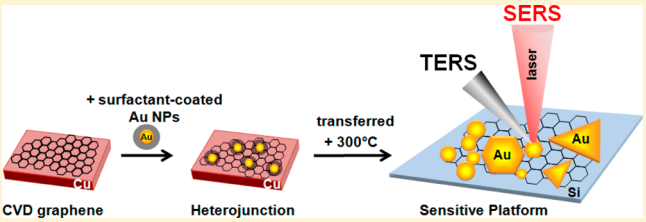

INTRODUCTION

The unique physicochemical properties of graphene combined with other nanoscale materials have already exceeded expectations about future applications in the area of nanomaterials science. Examples are the combination of graphene with hexagonal boron nitride (hBN) for proton separation membranes,[1] doped with N and B ions for opening the band gap in graphene,[2] deposition of a small amount of Co atoms for water splitting,[3] and formation of heterostructures with Au, Ag, and Cu NPs for dramatically improving Raman signals in SERS applications.[4] Even graphene combined with itself[5,6] in a bilayer or multilayer configuration has demonstrated to increase the band gap, therefore making it more suitable in the semiconductor industry.[7] The addition of metallic nanostructures to graphene is a smart approach toward the construction of SERS platforms, since graphene provides a vast surface area, while metallic centers improve Raman signal due to their plasmons. There are several interesting configurations of graphene with metal nanostructures[8,9] employed for the detection of low analyte concentrations[10−13] even down to a single molecule level[14] (SERS measurements) as well as exploring into local strain in graphene (i.e., tip-enhanced Raman spectroscopy, TERS).[8]

Few relevant methods for obtaining graphene were developed after the seminal isolation of graphene from graphite performed by Novoselov and Geim.[15] The chemical vapor deposition (CVD) is usually the chosen method because it yields to single layer graphene in a reproducible manner.[16] However, the transfer procedure involves the use of high molecular weight polymers such as poly(methyl-methacrylate) (PMMA), which cannot be completely removed from the nanocarbon.[17] The majority of approaches to remove PMMA have failed,[13,18] whereas successful ones required unpractical protocols involving, for instance, ion bombardment at controlled energy rates.[19] Our group recently demonstrated that employing conventional cleaning procedures[13] was not sufficient to completely remove polymer residues, as determined by changes in graphene conductivity and the appearance of Raman bands located at 1430 and 1550 cm^{-1} associated with impurities.[20] Transferring graphene without the use of polymers yields to a clean heterojunction readily for TERS and SERS studies.

Received: December 17, 2015
Revised: February 18, 2016
Published: February 19, 2016

DOI: 10.1021/acs.jpcc.5b12372
J. Phys. Chem. C 2016, 120, 8315−8322

Since the discovery of graphene, Raman spectroscopy has played a central role in characterizing 2D materials because it provides accurate information about the number of layers, film disorder, presence of impurities, and electronic state.[21] However, conventional Raman microscopy is a diffraction-limited technique. TERS, a technique that combines scanning probe microscopy (SPM) with Raman spectroscopy, delivers the same information as confocal Raman but improves by far local resolution.[22] Local resolution obtained by TERS is achieved by a combination of the dimensions of the nanoparticle (NP) probe that determines the spatial resolution, and its localized surface plasmons, which improves the sensitivity every time the tip approaches the sample. There are few effects that may cause changes in 2D band frequency of graphene, and those include the energy of the laser,[13,23] number of graphene layers,[15] electron or hole doping,[6] supported by a substrate[24] or suspended,[25] and local strain on graphene.[26,27] Local strain on graphene can either be induced by the tip,[27] detected by it,[28] or both[27] during near-field scanning. For instance, a decrease in frequency of the 2D band has been observed during tip scanning over ridges between graphene flakes grown on SiC,[29] between suspended and supported graphene,[25] and graphene deposited on a single 5 nm diameter Au nanoparticle.[8] All of these reports have shown a decrease in frequency and widening of the full width at half-maximum (fwhm) of the 2D band of graphene during TERS experiments.

Here, we report a simple but effective approach to transfer graphene employing surfactant-coated Au NPs. This approach benefits in two important aspects: (a) avoids the use of high molecular weight polymers (i.e., PMMA) and (b) incorporates Au NPs to team up with graphene toward the construction of hybrid nanomaterials with outstanding sensitivity. Those attributes led us to explore potential mismatch planes, local effects generated by Au NPs and Au tip, and SERS of rhodamine 6G (Rh6G) performed on different areas of single Au nanoplates and on Au NP networks at the heterojunction. TERS performed on NP networks showed reversible changes in frequency and fwhm of the 2D band every time the tip approached/retracted to/from the heterojunction. Surprisingly, SERS of Rh6G adsorbed onto a single Au triangular nanoplate indicated that the largest enhancement corresponds to the most irregular region from one particular border. These experiments reveal interesting information about the number of graphene layers, potential dislocation, doping as well as local strains in graphene as indicated by TERS.

EXPERIMENTAL METHODS

Chemicals. Sodium borohydride (99%), tetraoctylammonium bromide (99%), toluene (99.9%), ethanol (200 proof), acetone (99.9%), isopropyl alcohol (99.9%), $HAuCl_4$, rhodamine 6G (Rh6G) (Exciton), Cu foil (25 μm thick, 150 mm width × 90 m length, >99.99% MTI Corp.) were purchased from Aldrich Chemical Co. Gases of H_2 (99.999%) and CH_4 (99.999%) were purchased from Linde Argentina. $CuCl_2$ was synthesized from metallic Cu foil to the desired concentration. Milli-Q water (17.8 M cm) was employed for all aqueous solutions.

Synthesis of TOABr-Coated Au Nanoparticles (Au@TOABr). The TOABr-coated Au NPs (SNPs) were synthesized according to the two-phase Brust−Schiffrin reaction but without the addition of organic thiols.[30] Details of the synthesis were reported somewhere else. The nanoparticles prepared in this manner are 4.39 ± 1.25 and 2.96 ± 0.66 nm according to transmission electron microscopy (TEM)[31] and small-angle X-ray scattering (SAXS),[32] respectively.

Synthesis of Graphene by CVD. Graphene was grown by chemical vapor deposition (CVD) on a Cu foil previously sonicated three times 20 min each in acetone. Clean Cu foil was loaded into a quartz tube in a tube furnace pumped to 8.0×10^{-5} Torr. After reaching a steady pressure, 24 mL/min of H_2 was constantly passed through the tube during the entire growth process. The sample was then heated at 1000 °C for 30 min, and graphene was grown under a flow of CH_4 run at 75 mL/min for 5 min.[13,33] After removal from the furnace, the graphene was transferred to different substrates (Si, glass, and TEM grids) using the protocol described in the heterojunction formation.

PMMA-Free Graphene Transfer Procedure and Heterojunction Formation. The as-grown graphene was cut into small pieces (1 × 1 cm^2), placed in a Petri dish, and 40 μL of a concentrated solution of TOABr-Au NPs was drop-casted. The sample was allowed to air-dry and Cu foil removed with ∼5 mL of 2.0 M $CuCl_2$ (28% w/v) in 6 M of HCl mixed with isopropyl alcohol (10% v/v) which was carefully added to the Petri dish trying to avoid contact of the etching solution with the top layer of NPs. The Cu foil was completely dissolved in about 6 h. Finally, the etching solution was removed and replaced with a mixture of 10% v/v of isopropyl alcohol in water to remove the residual $CuCl_2$. This yields a heterojunction formed by TOABr-Au NPs films on top of graphene. The sample was then transferred to different substrates such as Si, glass, and Cu grids. The cleaned substrates (soaked in a solution of 10% (v/v) of IPA in water) were carefully immersed underneath the floating heterojunction (flakes of Au NPs/graphene) and pulled out from the solution to obtain the heterojunction.

Thermal Treatment. In order to remove the organic material from the Au NPs, the heterojunction was subjected to 300 °C for 1 h conducted in a Barnstead/Thermolyne Small Benchtop Muffle Furnaces Type 1300 (Thermo Scientific).

Microscopic Characterization. ***Raman experiments.*** Raman spectra were acquired in a LABRAM-HR Horiba Jobin-Yvon confocal microscope Raman system using a 632.8 nm (He−Ne) laser. Raman experiments were carried out with a 100× objective lens (0.9 NA) and 5.4 mW laser power. For SERS experiments, the heterojunction (graphene + Au nanoparticles) sample was immersed in 1.0×10^{-3} M Rh6G aqueous solution (pH 5). Excess Rh6G molecules were copiously rinsed with nanopure water. ***Raman imaging.*** Raman imaging was constructed by 64 Raman spectra collected by scanning every 0.5 μm along the entire triangular nanoplate. Acquisition time: 5 s for every 5 averaged spectrum. In this case, low laser power was used in order to avoid laser-induced heating (0.05 mW). ***TERS experiments.*** Tip-enhanced Raman scattering spectra were acquired in a Nanonics Imaging Ltd. Multiview 2000 microscope Scan Head Assembly (top-illumination) with a 100× objective lens (0.7 NA) optical fiber probe with a bent fiber tip coated with Cr. For each TERS experiment, the laser 632.8 nm (He−Ne) was carefully focused and locked onto the approached AFM tip, and the sample scanned underneath both. Au NP tips were purchased from Nanonics Imaging Ltd. ***AFM characterization.*** Atomic force microcopy images were acquired with the same microscope used for TERS using a Si tip operating in tapping mode at 30.62 kHz. ***HRTEM characterization.*** High resolution transmission electron microscopy (HRTEM) images were acquired with a Phillips CM 200 UT operated at 200 keV.

DOI: 10.1021/acs.jpcc.5b12372
J. Phys. Chem. C 2016, 120, 8315−8322

Spectroscopic Characterization. Scattering spectra were collected from individual Au nanoplates using resonant Rayleigh dark-field scattering spectroscopy. Bright-field and dark-field images were performed with an inverted Olympus microscope with a halogen lamp light source and a dark-field condenser (NA = 0.95−0.80) for sample illumination.

RESULTS AND DISCUSSION

PMMA-Free Transferred Graphene. The scheme in Figure 1 describes the three steps required for obtaining

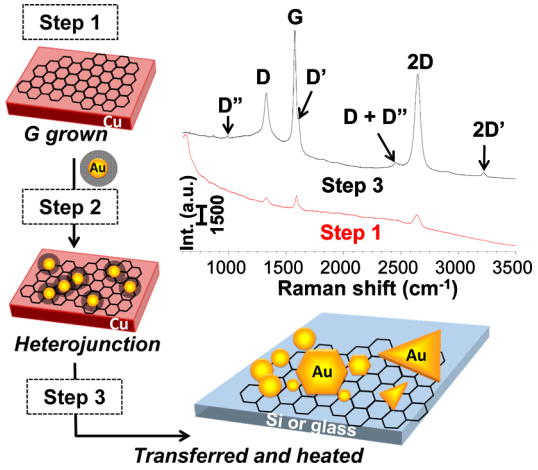

Figure 1. Scheme describes the general steps required for obtaining PMMA-free graphene. Step 1 involves graphene growth on a Cu foil by the CVD method followed by the heterojunction formation using surfactant-coated Au NPs (step 2), and finally Cu etching and transferring graphene to clean substrates prior to thermal treatment (step 3). The spectra exhibit Raman plots of as-synthesized graphene on Cu foil (step 1) and the heterojunction at step 3, as indicated.

PMMA-free graphene films. Step 1 shows CVD grown graphene on a Cu foil followed by drop casting tetraoctylammonium bromide (TOABr)-coated Au NPs (step 2) and Cu etching (see Methods section for more details). Thermal annealing causes an increase of the as-synthesized Au NP diameter from ∼3−4 nm[13,34] to ∼10 nm along with the formation of interesting Au features including nanoparticle networks, dimmers, and nanoplates of various shapes (circles, hexagons, and triangles), as indicated by wide field optical and HRTEM images shown in Figure 2. Figure S1 shows more HRTEM images of ∼10 nm diameter Au NPs associated with thermal annealing. Raman spectra were recorded on a selected area of graphene before (step 1) and after being transferred with Au NPs and thermally treated (step 3). Once transferring graphene, via Au NPs, is completed, the spectra exhibited ∼10-fold increase in intensity for all the characteristic graphene bands (D, G, and 2D) and the appearance of bands at ∼990 (D″), ∼1610 (D′), 2450 (D + D″), and ∼3220 cm^{-1} (2D′) (vide infra).[35] Importantly, the absence of bands at ∼1430, ∼1530, and ∼2900 cm^{-1} indicates that as-transferred and treated graphene lacks organic impurities either from polymers or alkyl chains.[17,20,36]

Parts A and B of Figure 2 show optical images of selected as-transferred areas corresponding to different shaped Au features and Au NP networks, respectively. Figure 2B exhibits an interesting Au NP network, which may have preferentially formed on grain boundaries of the graphene film. Parts C and D of Figure 2 and the inset exhibit HRTEM images of an as-

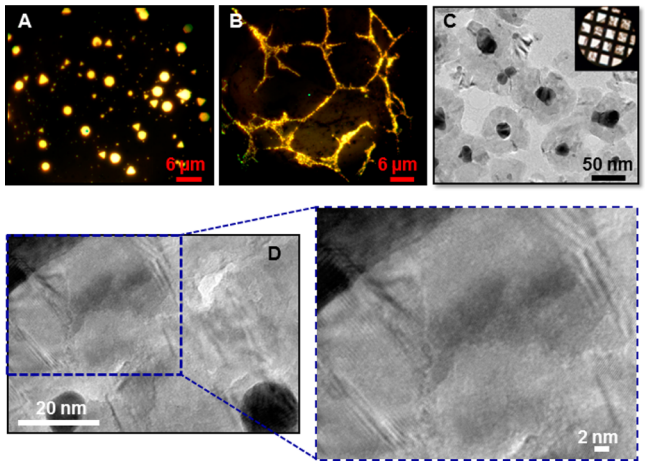

Figure 2. Optical (A, B) and HRTEM images (C, D) of selected as-transferred areas of the heterojunction on glass (A, B), which correspond to Au features of different shapes (A) and Au NP networks (B), the heterojunction on a Cu grid after thermal treatment (inset) showing Au NPs surrounded by some halo around the NPs (C), and shaded strips which may correspond to Moiré effects (D). The inset corresponds to a zoomed-in area from part D.

transferred and -treated heterojunction comprised of Au NPs surrounded by some shaded "halos" that may correspond to carbon allotropes. In addition, Figure 2D exhibits atomically arranged stripes along with shaded and bright spots which may indicate a Moiré pattern potentially caused by mismatch graphene planes.[37−39] It can also be attributed to carbon fragments (i.e., organic TOA^+ alkylchains) remaining after thermal treatment of Au NPs. However, Raman performed on the as-prepared heterojunction showed no evidence of $R-CH_2$ and $-CH_3$ stretching modes (i.e., Raman spectra in Figure 1), which should have indicated the presence of organic residues. The literature[39] recently have shown that, in the case of Moiré patterns, a Raman band should appear next to the G band, which is not observed here. As a result, a close examination into Raman bands in graphene and HRTEM revealed important information about the actual number of layers and potential dislocation between layers, respectively, whereas the presence of Au nanostructures teams up with graphene to significantly improve Raman sensitivity.

TERS Characterization. The PMMA-free transferring protocol and the formation of intriguing Au NPs networks lead us to explore mechanical strains in graphene. Figure 3 shows TERS measurements performed by successive movement of "tip up" and "tip down" on a selected Au NP network (aggregated area indicated in the inset). It should be noted that all the spectra and data shown in this figure were normalized to the intensity of the G band. In the far-field (tip retracted), the spectra exhibit the characteristic graphene bands corresponding to D, G, and 2D at ∼1325, ∼1585, and 2648 cm^{-1}, respectively. Note that these bands are observed despite the large concentration of Au NPs at the heterojunction. Each time the tip approaches the sample, a few interesting aspects should be addressed from the spectra as follows. First, all Raman modes reversibly change their wavenumbers and full width at half-maximum (fwhm). The blue shift (higher wavenumbers) observed for the D and 2D bands suggests that the system requires higher energy to excite vibrational modes in graphene (vide infra). Second, outstanding spatial resolution led to the exaltation of former bands (i.e., disorder D band) along with

DOI: 10.1021/acs.jpcc.5b12372
J. Phys. Chem. C 2016, 120, 8315−8322

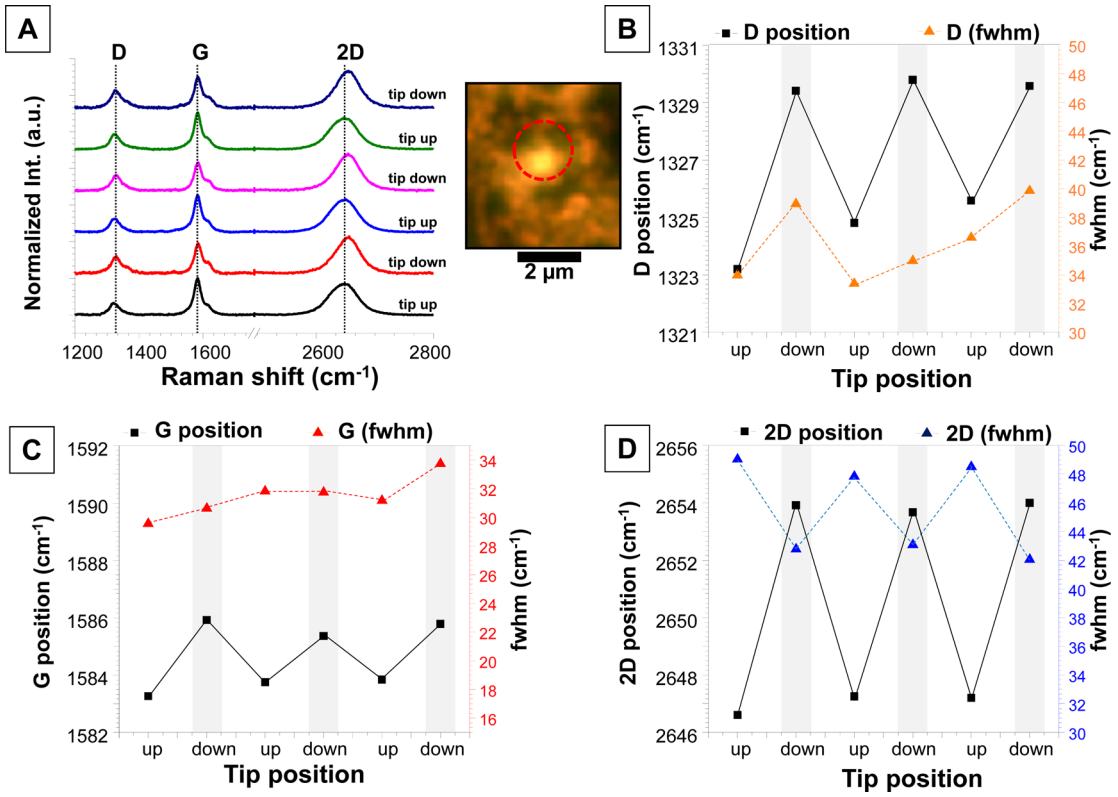

Figure 3. TERS characterization at "tip up" and "tip down" conditions, performed on a selected Au NPs network as indicated by the optical image next to part A (A). Plots are offset for better comparison. All of the spectra and data shown were normalized to the intensity of the G band. Change in frequency and fwhm of the D (B), G (C), and 2D (D) bands during "tip up/tip down" experiments corresponding to the plots shown in part A, as indicated. The black lines and gray shadows are guides for the eye.

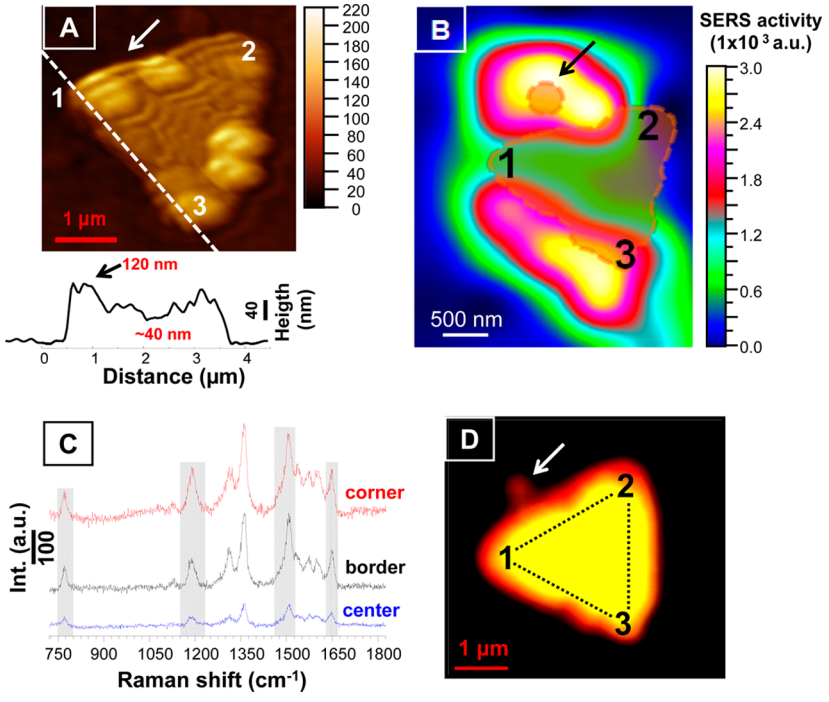

Figure 4. Tapping mode AFM image along with a cross-section of the triangular nanoplate exhibiting different heights along the border of the nanoplate ranging from 40 to 120 nm (A). The arrow points out a region where the reference NP used to be before AFM scanning. The Raman image shows a color chart constructed by Raman measurements acquired at 760 cm^{-1} (B). Representative Raman plots of Rh6G measured at corners, borders, and center as indicated (C). Shaded strips represent four of the characteristics Raman bands of Rh6G. Optical image with exalted colors labeled with 1, 2, and 3 corresponding to corners of the same nanoplate (D).

DOI: 10.1021/acs.jpcc.5b12372
J. Phys. Chem. C 2016, 120, 8315−8322

better resolved bands D′ (~1610 cm^{-1}) and D + D′ (~2920 cm^{-1}) which are not observed in the retracted position (see also Figure S2). The D′ band is activated by a single-phonon intravalley scattering process[35,40,41] also affected by defects or faults in graphene, whereas the D + D′ is a combination of both.[41] Finally, Figure 3B, C, and D show plots of frequency (and fwhm) versus number of successive tip events (tip up and down) accounted for the D, G, and 2D bands, respectively. The shift observed for the 2D band (8−10 cm^{-1}), as expected, is twice that of the D band (4−5 cm^{-1}), since the former is an intervalley double-phonon resonance process.[35] The frequency of the G band increases to a lesser extent (2−3 cm^{-1}) relative to any of the other two bands. Changes in the fwhm are also observed for all the bands involved in this study; however, they follow different trends. For instance, the 2D band fwhm reversibly increases/decreases as long as the tip is up/down, while G and D bands progressively increase regardless of the tip position. Figure S2 shows TERS results obtained from another Au NP network of the sample indicating a reproducible behavior.

To the best of our knowledge, there is just one report by Novotny and co-workers[8] who performed TERS on a heterojunction formed by NPs and graphene. They scanned over a single Au nanoparticle placed underneath a mechanically exfoliated graphene and observed a decrease in frequency and fwhm during TERS scanning. Their heterojunction resembles ours in the sense that it combines Au NPs with graphene; however, the configuration is different, since the tip is scanning directly on graphene instead of Au NPs. That could be one reason why their results, in terms of frequency, opposed ours by decreasing instead of increasing. We believe that the shift of the 2D band to higher frequency can be associated with electron transfer from graphene to the Au tip.[42] Figure S3 shows a control experiment performed in an as-transferred area of the sample where the Raman image exhibits no Au features or networks. The figure shows a TERS plot and table for tip down and up positions indicating that D, G, and 2D wavenumbers followed a similar paradigm (blue-shifted) as that observed in Figure 3A and Figure S2. This effect can be associated with local doping which turns graphene into a p-type (majority of hole carriers) nanocarbon as a result of electron withdrawing.[43] It can be further confirmed by systematic changes in frequency of the G band also associated with changes in the Fermi level.[44] More experiments are underway in order to conclusively determine this behavior.

SERS Activity on a Single Triangle Nanoplate. In order to test SERS activity on a single nanostructure, the as-transferred graphene sample was immersed in 1 × 10^{-3} M Rh6G aqueous solution for 60 min. We performed Raman spectroscopy and AFM (cross-section profiles and RMS values) on each corner, border, and center of a single triangular nanoplate. Figure 4A shows a tapping mode AFM image of the nanoplate along with its cross-section profile measured at a particular border, labeled 1−3 (cross-sections from other areas are shown in Figure S4). The arrow points out a spot where there used to be a NP, used as a reference, before AFM scanning. The cross-section along that particular border reveals a significant difference in thickness ranging from ~40 to ~120 nm. Figure 4B shows a Raman image of SERS intensity from Rh6G molecules measured at 760 cm^{-1}, which corresponds to in-plane C−C−C ring bending[45] (for more details, see the Experimental Section). As shown in Figure 4B, the Raman image reveals a nonuniform distribution of Rh6G SERS signal consistent with 1 order of magnitude difference between the center and border of the nanoplate. This difference in the Raman signal can be associated with nonuniform electromagnetic fields along the entire surface of the nanoplate. There are numerous reports on SERS caused by nanoparticles smaller than 100 nm, where the enhancement is associated with localized surface plasmon resonance.[46] However, differences in Raman intensity cannot be observed experimentally at different points of the individual nanoparticle because the SERS resolution is limited by diffraction. On the other hand, when working with extended substrates such as a nanoprism,[47] increased Raman signal is usually attributed to variations in surface roughness.

In this work, we have studied a single nanoplate with intermediate characteristics between small particles and a rough extended surface, i.e., observable plasmonic modes (see Figure S5). The scattering spectrum of this particular nanoplate indicates that the Stokes fingerprint of Rh6G falls within the range of one of the plasmonic modes of the Au nanoplate. This result suggests that electromagnetic effects may also contribute to Raman enhancement of Rh6G. However, it can also be attributed to differences in the surface roughness of the nanoplate, as can be seen in the AFM image and root-mean-square (RMS) values (Table 1).

Table 1. Correlation between Enhancement Factor (EF), Root Mean Square (RMS), and Thickness Range Taken from Corners, Borders, and the Center of the Nanoplate

area of the nanoplate	EF[a] (×10^3)	RMS[b] (nm)	thickness range[c] (nm)
corner 1	0.3	32.8	
corner 2	0.4	11.9	
corner 3	3.0	18.2	
border 1−3	2.5	23.3	40−120
border 1−2	1.7	28.2	70−130
border 2−3	0.2	28.6	80−160
center	0.6	4.9	90−120

[a]Corresponds to the enhanced factor (EF) values of Rh6G measured at 760 cm^{-1} for different areas of the nanoplate with respect to the Rh6G intensity measured outside of the nanoplate. [b]Root-mean-square (RMS) roughness values. [c]Thickness range obtained by cross-sections in different areas, as indicated here and in Figure 4A and Figure S3. *Note that corner 3 possess a nanoparticle on top consistent with the largest RMS value (most irregular) of the nanoplate.

We believe that the reference NP shown in the optical image of Figure 4D, in close proximity to border 1−2, may have influenced the electromagnetic field distribution in this area, as it is clearly shown in the Raman image. For this reason, we centered our analysis in all the areas of the nanoplate but excluded border 1−2 for a fair comparison. Figure 4C shows three Raman spectra of Rh6G adsorbed on the selected regions within the nanoplate. The less intense SERS spectrum comes from the central part of the nanoplate, with a Raman enhancement factor (EF) of ~0.6 × 10^3. Values of EF measured at border 1−3 and corner 3 are 2.5 × 10^3 and 3.0 × 10^3, respectively, consistent with larger Raman intensity. This behavior can be rationalized in terms of the difference in the surface roughness for these regions of the nanoplate. Table 1 summarizes a correlation between EF, RMS, and thickness range taken from corners, borders, and the center of the nanoplate. The table shows that the RMS value at the center is

DOI: 10.1021/acs.jpcc.5b12372
J. Phys. Chem. C 2016, 120, 8315−8322

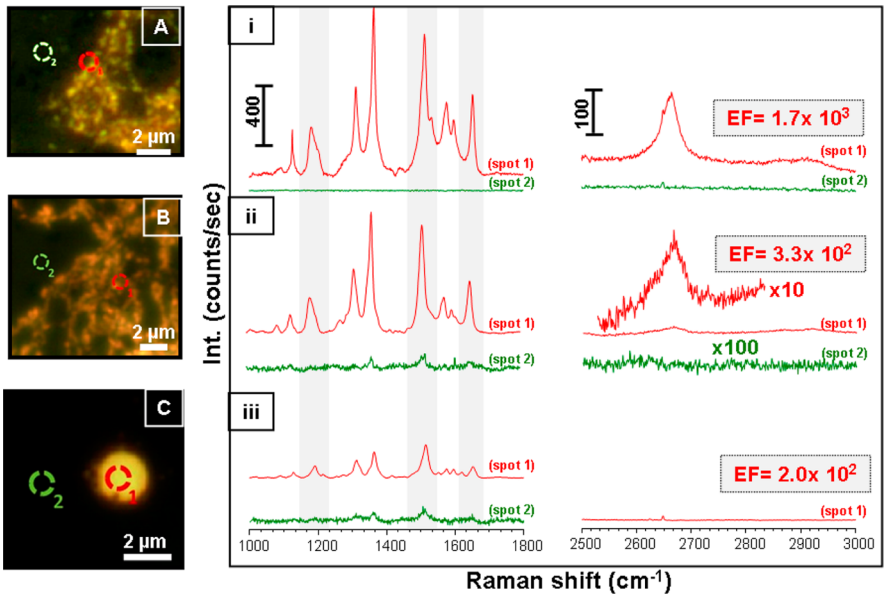

Figure 5. Optical images (A, B, and C) and corresponding SERS (i, ii, and iii) of Rh6G recorded on three different areas of the same heterojunction, including two different Au NP networks (different aggregated areas) (A, B) and a single circular nanoplate (C). Enhanced factor (EF) values of Rh6G measured at 1362 cm^{-1} are also indicated. The red (1) and green (2) circles indicate the laser spot focused inside and outside the heterojunction, respectively. For clarity, the spectra were separated into two panels with different intensity scales.

4× lower than those in the border and corner, whereas borders and corners are quite similar between them. In conclusion, the spatially modulated SERS signal observed can be attributed to two predominant factors such as electromagnetic effects and differences in surface roughness along the nanoplate.

SERS Activity on Au NP Networks. We expanded SERS studies to other Au NP configurations formed on the sample, such as Au NP networking (Figure 5A and B) and regions with a single circular Au nanoplate (Figure 5C). Comparison of SERS spectra from two NP networks indicates almost 1 order of magnitude difference in the intensity of Rh6G between Figure 5A (EF = 1.7 × 10^3) and Figure 5B (EF = 3.3 × 10^2). The optical image in Figure 5A shows more crowded and well-defined Au NPs as compared to the other network observed which may be responsible for improving the Raman signal. It is not surprising, though, that the electromagnetic field between particles is notably increased when the distance between them is diminished, giving higher EF values.[47] As in the Raman spectrum from Figure 1, it should be noted that the 2D band is not completely shielded by Au NPs at the heterojunction. It is also worth noticing in Figure 5iii a small spike corresponding to the 2D band, which persists despite the presence of a thick Au nanoplate. It is reasonable to think that Au may act as an antenna of energy propagation as recently demonstrated with Au nanorods placed on graphene.[48] Further experiments will be conducted in order to test the ability of the heterojunction to propagate energy to greater depths.

CONCLUSIONS

In conclusion, transferring graphene using surfactant-coated Au NPs instead of polymers benefited in two important aspects. First, the heterojunction was free from impurities which is a highly required condition given by SERS and TERS. Second, annealing of the heterojunction led to interesting Au features (NPs networks, triangular and circular nanoplates, etc.), which acted as ideal TERS and SERS platforms. Raman and HRTEM results denote the presence of bilayer graphene and potential dislocation between them, respectively. In this heterojunction, TERS results suggested that Au might be responsible for withdrawing electrons from graphene, as evidenced by the higher energy needed to excite those Raman bands (phonon). SERS performed on a single triangular-shape nanoplate demonstrated that borders have larger EF of Rh6G than corners and strikingly larger than the center likely due to surface roughness and irregular areas of the nanoplate. A close examination into aggregated Au NPs and a circular nanoplate exhibited that crowded areas and well-defined nanoparticles on graphene are better SERS platforms rather than a flat circular nanoplate. We will further explore TERS of individual nanoplates and the propagation of phonons in the heterojunction (metal + graphene).

ASSOCIATED CONTENT

Supporting Information

The Supporting Information is available free of charge on the ACS Publications website at DOI: 10.1021/acs.jpcc.5b12372.

High resolution transmission electron microcopy (HRTEM) images of Au nanoparticles at the heterojunction; TERS spectra of heterojunctions both in an area with and without Au NP networks, along with tables showing the Lorentz fit performed to all the characteristic Raman bands; AFM images (tapping mode) and cross-sections of the triangular nanoplates measured along the center and borders; bright- and dark-field microscopy images of a heterojunction on a glass substrate; scattering spectrum of a single triangular Au nanoplate (PDF)

AUTHOR INFORMATION

Corresponding Authors

*E-mail: glacconi@mail.fcq.unc.edu.ar.

*E-mail: fjiban@inifta.unlp.edu.ar. Phone: +54 (221) 425 7430/7296- Int: 179. Fax: +54 (221) 425 4642.

DOI: 10.1021/acs.jpcc.5b12372
J. Phys. Chem. C 2016, 120, 8315−8322

Notes

The authors declare no competing financial interest.

■ ACKNOWLEDGMENTS

We gratefully acknowledge financial support from projects PIP-0917 (CONICET), SECyT-UNC. M.C.D. acknowledges Pablo S. Fernández (Chemistry Institute (IQ)-University of Campinas, Brazil) and Matías F. Calderón (INIFTA) for helping during graphene synthesis and sample preparations. Raman microscopy facilities were supported by Laboratorio de Nanoscopía y Nanofotónica LANN-SNM of MINCyT (PME 1544) at INFIQC-CONICET.

■ REFERENCES

(1) Hu, S.; Lozada-Hidalgo, M.; Wang, F. C.; Mishchenko, A.; Schedin, F.; Nair, R. R.; Hill, E. W.; Boukhvalov, D. W.; Katsnelson, M. I.; Dryfe, R. A. W.; et al. Proton Transport Through One-Atom-Thick Crystals. *Nature* **2014**, *516*, 227−230.

(2) Telychko, M.; Mutombo, P.; Merino, P.; Hapala, P.; Ondráček, M.; Bocquet, F. C.; Sforzini, J.; Stetsovych, O.; Vondráček, M.; Jelínek, P.; et al. Electronic and Chemical Properties of Donor, Acceptor Centers in Graphene. *ACS Nano* **2015**, *9*, 9180−9187.

(3) Fei, H.; Dong, J.; Arellano-Jimenez, M. J.; Ye, G.; Dong Kim, N.; Samuel, E. L. G.; Peng, Z.; Zhu, Z.; Qin, F.; Bao, J.; et al. Atomic Cobalt on Nitrogen-Doped Graphene for Hydrogen Generation. *Nat. Commun.* **2015**, *6*, 8668.

(4) Wei, H.; Xu, H. Hot Spots in Different Metal Nanostructures for Plasmon-Enhanced Raman Spectroscopy. *Nanoscale* **2013**, *5*, 10794−10805.

(5) Jorio, A.; Saito, R.; Dresselhaus, M. S.; Dresselhaus, G. *Raman Spectroscopy in Graphene Related Systems*; Wiley Vch Verlag Gmbh: Weinheim, Germany, 2011.

(6) Shinde, P. P.; Kumar, V. SEMICONDUCTING GRAPHENE. *Nano LIFE* **2012**, *02*, 1230009.

(7) Bao, Q.; Loh, K. P. Graphene Photonics, Plasmonics, and Broadband Optoelectronic Devices. *ACS Nano* **2012**, *6*, 3677−3694.

(8) Beams, R.; Cançado, L. G.; Jorio, A.; Vamivakas, A. N.; Novotny, L. Tip-Enhanced Raman Mapping of Local Strain in Graphene. *Nanotechnology* **2015**, *26*, 175702.

(9) Pashaee, F.; Sharifi, F.; Fanchini, G.; Lagugné-Labarthet, F. Tip-Enhanced Raman Spectroscopy of Graphene-like and Graphitic Platelets on Ultraflat Gold Nanoplates. *Phys. Chem. Chem. Phys.* **2015**, *17*, 21315−21322.

(10) Xu, W.; Ling, X.; Xiao, J.; Dresselhaus, M. S.; Kong, J.; Xu, H.; Liu, Z.; Zhang, J. Surface Enhanced Raman Spectroscopy on a Flat Graphene Surface. *Proc. Natl. Acad. Sci. U. S. A.* **2012**, *109*, 9281.

(11) Murphy, S.; Huang, L.; Kamat, P. V. Reduced Graphene Oxide−Silver Nanoparticle Composite as an Active SERS Material. *J. Phys. Chem. C* **2013**, *117*, 4740−4747.

(12) Xu, S.; Man, B.; Jiang, S.; Wang, J.; Wei, J.; Xu, S.; Liu, H.; Gao, S.; Liu, H.; Li, Z.; et al. Graphene/Cu Nanoparticle Hybrids Fabricated by Chemical Vapor Deposition As Surface-Enhanced Raman Scattering Substrate for Label-Free Detection of Adenosine. *ACS Appl. Mater. Interfaces* **2015**, *7*, 10977−10987.

(13) Dalfovo, M. C.; Lacconi, G. I.; Moreno, M.; Yappert, M. C.; Sumanasekera, G. U.; Salvarezza, R. C.; Ibañez, F. J. Synergy Between Graphene and Au Nanoparticles (Heterojunction) Towards Quenching, Improving Raman Signal, and UV Light Sensing. *ACS Appl. Mater. Interfaces* **2014**, *6*, 6384−6391.

(14) Wang, P.; Liang, O.; Zhang, W.; Schroeder, T.; Xie, Y.-H. Ultra-Sensitive Graphene-Plasmonic Hybrid Platform for Label-Free Detection. *Adv. Mater.* **2013**, *25*, 4918−4924.

(15) Ferrari, A. C.; Meyer, J. C.; Scardaci, V.; Casiraghi, C.; Lazzeri, M.; Mauri, F.; Piscanec, S.; Jiang, D.; Novoselov, K. S.; Roth, S.; et al. Raman Spectrum of Graphene and Graphene Layers. *Phys. Rev. Lett.* **2006**, *97*, 187401.

(16) Li, X.; Zhu, Y.; Cai, W.; Borysiak, M.; Han, B.; Chen, D.; Piner, R. D.; Colombo, L.; Ruoff, R. S. Transfer of Large-Area Graphene Films for High-Performance Transparent Conductive Electrodes. *Nano Lett.* **2009**, *9*, 4359−4363.

(17) Lin, Y.-C.; Lu, C.-C.; Yeh, C.-H.; Jin, C.; Suenaga, K.; Chiu, P.-W. Graphene Annealing: How Clean Can It Be? *Nano Lett.* **2011**, *12*, 414−419.

(18) Pirkle, A.; Chan, J.; Venugopal, A.; Hinojos, D.; Magnuson, C. W.; McDonnell, S.; Colombo, L.; Vogel, E. M.; Ruoff, R. S.; Wallace, R. M. The Effect of Chemical Residues on the Physical and Electrical Properties of Chemical Vapor Deposited Graphene Transferred to SiO2. *Appl. Phys. Lett.* **2011**, *99*, 122108.

(19) Lim, Y.-D.; Lee, D.-Y.; Shen, T.-Z.; Ra, C.-H.; Choi, J.-Y.; Yoo, W. J. Si-Compatible Cleaning Process for Graphene Using Low-Density Inductively Coupled Plasma. *ACS Nano* **2012**, *6*, 4410−4417.

(20) Lin, Y.-C.; Jin, C.; Lee, J.-C.; Jen, S.-F.; Suenaga, K.; Chiu, P.-W. Clean Transfer of Graphene for Isolation and Suspension. *ACS Nano* **2011**, *5*, 2362−2368.

(21) Pimenta, M. A.; del Corro, E.; Carvalho, B. R.; Fantini, C.; Malard, L. M. Comparative Study of Raman Spectroscopy in Graphene and MoS2-Type Transition Metal Dichalcogenides. *Acc. Chem. Res.* **2015**, *48*, 41−47.

(22) Stadler, J.; Schmid, T.; Zenobi, R. Developments in and Practical Guidelines for Tip-Enhanced Raman Spectroscopy. *Nanoscale* **2012**, *4*, 1856−1870.

(23) Costa, S. D.; Righi, A.; Fantini, C.; Hao, Y.; Magnuson, C.; Colombo, L.; Ruoff, R. S.; Pimenta, M. A. Resonant Raman Spectroscopy of Graphene Grown on Copper Substrates. *Solid State Commun.* **2012**, *152*, 1317−1320.

(24) Wang, Y. y.; Ni, Z. h.; Yu, T.; Shen, Z. X.; Wang, H. m.; Wu, Y. h.; Chen, W.; Shen Wee, A. T. Raman Studies of Monolayer Graphene: The Substrate Effect. *J. Phys. Chem. C* **2008**, *112*, 10637−10640.

(25) Reserbat-Plantey, A.; Kalita, D.; Han, Z.; Ferlazzo, L.; Autier-Laurent, S.; Komatsu, K.; Li, C.; Weil, R.; Ralko, A.; Marty, L.; et al. Strain Superlattices and Macroscale Suspension of Graphene Induced by Corrugated Substrates. *Nano Lett.* **2014**, *14*, 5044−5051.

(26) Snitka, V.; Rodrigues, R. D.; Lendraitis, V. Novel Gold Cantilever for Nano-Raman Spectroscopy of Graphene. *Microelectron. Eng.* **2011**, *88*, 2759−2762.

(27) Wang, P.; Zhang, D.; Li, L.; Li, Z.; Zhang, L.; Fang, Y. Reversible Defect in Graphene Investigated by Tip-Enhanced Raman Spectroscopy. *Plasmonics* **2012**, *7*, 555−561.

(28) Shiotari, A.; Kumagai, T.; Wolf, M. Tip-Enhanced Raman Spectroscopy of Graphene Nanoribbons on Au(111). *J. Phys. Chem. C* **2014**, *118*, 11806−11812.

(29) Vantasin, S.; Tanabe, I.; Tanaka, Y.; Itoh, T.; Suzuki, T.; Kutsuma, Y.; Ashida, K.; Kaneko, T.; Ozaki, Y. Tip-Enhanced Raman Scattering of the Local Nanostructure of Epitaxial Graphene Grown on 4H-SiC $(000\bar{1})$. *J. Phys. Chem. C* **2014**, *118*, 25809−25815.

(30) Fink, J.; Kiely, C. J.; Bethell, D.; Schiffrin, D. J. Self-Organization of Nanosized Gold Particles. *Chem. Mater.* **1998**, *10*, 922−926.

(31) Dalfovo, M. C.; Salvarezza, R. C.; Ibañez, F. J. Improved Vapor Selectivity and Stability of Localized Surface Plasmon Resonance with a Surfactant-Coated Au Nanoparticles Film. *Anal. Chem.* **2012**, *84*, 4886−4892.

(32) Dalfovo, M. C.; Giovanetti, L. J.; Ramallo-López, J. M.; Salvarezza, R. C.; Requejo, F. G.; Ibañez, F. J. Real-Time Monitoring Distance Changes in Surfactant-Coated Au Nanoparticle Films Upon Volatile Organic Compounds (VOCs). *J. Phys. Chem. C* **2015**, *119*, 5098−5106.

(33) Sidorov, A. N.; Sherehiy, A.; Jayasinghe, R.; Stallard, R.; Benjamin, D. K.; Yu, Q.; Liu, Z.; Wu, W.; Cao, H.; Chen, Y. P.; et al. Thermoelectric Power of Graphene as Surface Charge Doping Indicator. *Appl. Phys. Lett.* **2011**, *99*, 013115.

(34) Fink, J.; Kiely, C. J.; Bethell, D.; Schiffrin, D. J. Self-Organization of Nanosized Gold Particles. *Chem. Mater.* **1998**, *10*, 922−926.

(35) Venezuela, P.; Lazzeri, M.; Mauri, F. Theory of Double-Resonant Raman Spectra in Graphene: Intensity and Line Shape of

DOI: 10.1021/acs.jpcc.5b12372
J. Phys. Chem. C 2016, 120, 8315−8322

Defect-Induced and Two-Phonon Bands. *Phys. Rev. B: Condens. Matter Mater. Phys.* **2011**, *84*, 035433.
(36) Schmid, T.; Opilik, L.; Blum, C.; Zenobi, R. Nanoscale Chemical Imaging Using Tip-Enhanced Raman Spectroscopy: A Critical Review. *Angew. Chem., Int. Ed.* **2013**, *52*, 5940−5954.
(37) Tománek, D.; Louie, S. G.; Mamin, H. J.; Abraham, D. W.; Thomson, R. E.; Ganz, E.; Clarke, J. Theory and Observation of Highly Asymmetric Atomic Structure in Scanning-Tunneling-Microscopy Images of Graphite. *Phys. Rev. B: Condens. Matter Mater. Phys.* **1987**, *35*, 7790−7793.
(38) N'Diaye, A. T.; Coraux, J.; Plasa, T. N.; Busse, C.; Michely, T. Structure of Epitaxial Graphene on Ir(111). *New J. Phys.* **2008**, *10*, 043033.
(39) Carozo, V.; Almeida, C. M.; Ferreira, E. H. M.; Cançado, L. G.; Achete, C. A.; Jorio, A. Raman Signature of Graphene Superlattices. *Nano Lett.* **2011**, *11*, 4527−4534.
(40) Basko, D. M. Theory of Resonant Multiphonon Raman Scattering in Graphene. *Phys. Rev. B: Condens. Matter Mater. Phys.* **2008**, *78*, 125418.
(41) Eckmann, A.; Felten, A.; Mishchenko, A.; Britnell, L.; Krupke, R.; Novoselov, K. S.; Casiraghi, C. Probing the Nature of Defects in Graphene by Raman Spectroscopy. *Nano Lett.* **2012**, *12*, 3925−3930.
(42) Wang, Y.; Ni, Z.; Hu, H.; Hao, Y.; Wong, C. P.; Yu, T.; Thong, J. T. L.; Shen, Z. X. Gold on Graphene as a Substrate for Surface Enhanced Raman Scattering Study. *Appl. Phys. Lett.* **2010**, *97*, 163111-1−163111-3.
(43) Klusek, Z.; Dabrowski, P.; Kowalczyk, P.; Kozlowski, W.; Olejniczak, W.; Blake, P.; Szybowicz, M.; Runka, T. Graphene on Gold: Electron Density of States Studies by Scanning Tunneling Spectroscopy. *Appl. Phys. Lett.* **2009**, *95*, 113114.
(44) Beams, R.; Gustavo Cançado, L.; Novotny, L. Raman Characterization of Defects and Dopants in Graphene. *J. Phys.: Condens. Matter* **2015**, *27*, 083002.
(45) Majoube, M.; Henry, M. Fourier Transform Raman and Infrared and Surface-Enhanced Raman Spectra for Rhodamine 6G. *Spectrochim. Acta Part Mol. Spectrosc.* **1991**, *47*, 1459−1466.
(46) Lin, W.-H.; Lu, Y.-H.; Hsu, Y.-J. Au Nanoplates as Robust, Recyclable SERS Substrates for Ultrasensitive Chemical Sensing. *J. Colloid Interface Sci.* **2014**, *418*, 87−94.
(47) Brus, L. Noble Metal Nanocrystals: Plasmon Electron Transfer Photochemistry and Single-Molecule Raman Spectroscopy. *Acc. Chem. Res.* **2008**, *41*, 1742−1749.
(48) Alonso-González, P.; Nikitin, A. Y.; Golmar, F.; Centeno, A.; Pesquera, A.; Vélez, S.; Chen, J.; Navickaite, G.; Koppens, F.; Zurutuza, A.; et al. Controlling Graphene Plasmons with Resonant Metal Antennas and Spatial Conductivity Patterns. *Science* **2014**, *344*, 1369−1373.

DOI: 10.1021/acs.jpcc.5b12372
J. Phys. Chem. C 2016, 120, 8315−8322